Optik - International Journal for Light and Electron Optics 243 (2021) 167490

Contents lists available at ScienceDirect

Optik

journal homepage: www.elsevier.com/locate/ijleo

Anisotropic optical properties of $Cu_2ZnSn(S_xSe_{1-x})_4$ solid solutions: First-principles calculations with TB-mBJ+U

Mohamed Issam Ziane [a,*], Hamza Bennacer [b], Mohammed Mostefaoui [c], Meftah Tablaoui [d], Moufdi Hadjab [b], Abdelkader Saim [e], Kheira Bekhedda [d]

[a] Higher School in Electrical and Energetic Engineering (ESGEE), Oran 31000, Algeria
[b] University of M'sila, M'sila 28000, Algeria
[c] LabRI-SBA Lab., Ecole Supérieure en Informatique (ESI), Sidi Bel Abbes 22000, Algeria
[d] Research Center in Semiconductor Technologies for Energetic (CRTSE), 02 Bd Frantz Fanon, BP. 140 Algiers, Algeria
[e] Laboratoire d'Electronique d'Electromagnétisme de photonique et d'Optique, Université Djillali Liabes de Sidi Bel Abbes, 22000 Sidi Bel Abbes, Algeria

ARTICLE INFO

Keywords:
TB-mBJ+U
CZTSSe
Stannite
Band gap
Absorption coefficient

ABSTRACT

The main aim of this work is to determine and explain the relationships between optoelectronic properties and the sulfur anion content in $Cu_2ZnSn(S_xSe_{1-x})_4$ solid solution. Band gap and absorption coefficient are of primary interest to the engineers and scientists researcher worked in optoelectronic field. Herein, the electronic and optical properties are calculated based on 128 conventional atoms within lattice parameters obtained at 300 K by using the FP-LAPW method combined with quasi-harmonic Debye model. The composition dependent band gaps of CZTSSe solid solutions are investigated by TB-mBJ+U. As results, all materials are semiconductors with a direct band gap ranging from 0.614 to 0.99 eV. The band gap variation increases as a function of sulfur anion content and showed a positive deviation from Vegard's law with a very small downward bowing parameter of + 0.079 eV. The density of state (DOS) calculations indicate that the energy bands of VBM involve Cu_d/anion(S/Se)_p hybridized antibonding-like states. Based on band alignment, the Ec offset between CZTS and CZTSe is larger than the Ev offset. These results are reported previously in other work and are confirmed in this study. Our work included a systematic comparison of the influence of S/(S+Se) atomic ratios on optical quantities. The dielectric function tensors show remarkable anisotropy. In addition, the static dielectric constants are found to decrease with sulfur anion content. The CZTSSe is proved to be suitable for good solar cells with high absorption coefficient ($> 10^4$ cm^{-1}). Such deep optical studies would be helpful for future optoelectronic applications of these compounds with different S/(S+Se) atomic ratios.

1. Introduction

Due to the development of industry, transport and communications sectors, world demand in electricity consumption has been observed in recent decades. However, till now the most of the electrical energy is produced by non-renewable combustion resources (such as oil, gas, nuclear). The development of renewable and clean energy sources is therefore timely. The Renewable energy sources

* Corresponding author.
E-mail address: issam1308@yahoo.fr (M.I. Ziane).

https://doi.org/10.1016/j.ijleo.2021.167490
Received 10 July 2020; Received in revised form 11 June 2021; Accepted 18 June 2021
Available online 22 June 2021

include wind, marine and ocean flows, geothermal energy, and solar photovoltaic. The latter is a very powerful source of energy, where the electricity is obtained directly by transformation of sunlight into electricity through a photovoltaic cell. This production of electricity by photovoltaic conversion occurs within semiconductor materials, that they have the properties to release their charge carriers (electron and hole) after absorption of photons from sunlight. That is why, research efforts are running for the development of solar cell from abundant and less toxic elements.

For more than thirty years, the materials based chalcogenides, especially Cu_2ZnSnS_4 (CZTS) quaternary compounds have been intensively studied for photovoltaic applications by virtue of its good electrical characteristics, earth-abundant and low cost mass production [1,2]. In 1988, Ito and co-author from Shinshu university, deposited thin films of CZTS stannite-type on heated glass substrates using atom beam sputtering [3] resulting in high absorption coefficient larger than 10^4 cm^{-1} and a band gap of 1.45 eV that corresponds to the optimum band gap energy for photovoltaic solar cell application. The best CZTS cell exhibited a conversion efficiency of 9.4% in the active area with CdS as the buffer layer [4]. Among the new other materials considered for photovoltaic, which is an outsider to CZTS is the $Cu_2ZnSnSe_4$ (CZTSe). The CZTSe compounds are structural analogue to CZTS and do not consist of any rare-metal such as In and Ga. Owing to its tunable direct electronic band gap and adequate optical and electrical properties, the latter has also garnered significant attention as photoactive materials in solar cell applications. Several experimentally and theoretical studies confirmed the dramatic fall in the band gap energy from ~1.45 to ~1 eV by subsiding the concentration of sulfur (S) with selenium (Se) [5–9]. Brammertz et al. [10] have demonstrated record cell efficiency of 9.7% with thin film solar cell based on $Cu_2ZnSnSe_4$-CdS-ZnO.

Other members of chalcogenide family, like CZTSSe materials, were discovered shortly after. The quinary solid solution $Cu_2ZnSn(S_xSe_{1-x})_4$ have been the focus of several research as it holds presents the advantage of being electrically and optically tunable due to its mixture of both S and Se. The solid solution exhibits a direct band gap, over the range 1.0–1.5 eV by decreasing the sulfur (S) content, which permits to obtain rather large light conversion efficiency when it will be placed as an absorbent layer in thin-film solar cells. The CZTSSe cell efficiency of 8.25% has been reported by Liu et al. [11], 9.02% by Wu et al. in 2015 [12], 9.2% by Carter et al. [13], 9.7% by Larsen et al. [14], 10.1% by Barkhouse et al. [15], 12.3% by introducing the chalcogenization source material SeS_2 during the annealing process [16], and the highest one of 12.6% was reported in 2013 by Wang et al. [17].

It is noteworthy that, the quaternary compounds such as CZTS and CZTSe are semiconductor materials of group I_2-II-IV-VI_4 and manifest in two different types of space group; I-4 Kesterite (Ks) or I-42 m Stannite (St). The difference between St and Ks structures is on the occupancy of the 2a(000) Wyckoff position: Zn elements in St and Cu in Ks [18].

The CZTSSe diamond-like materials containing two chalcogenide elements (Sulfur and Selenium) as a substantial constituent and have also tetrahedral coordinated crystal structures characterized by tetrahedral bonding, every atom in the structure has four nearest neighbors [19]. The experimentally results obtained by Keng-Liang et al. [20] and Nagaoka et al. [21] revealed that the solid solution $Cu_2ZnSn(S_xSe_{1-x})_4$ with different x compositions exhibited a stannite structure with I-42 m as space group.

The use such a material in such photovoltaic application or other goes through a great investigation on their electronic structure. Our attention focused on the mixture of two chalcogens S and Se, which is the subject of many studies including photovoltaic applications. In this present paper, the electronic and optical properties of the Stannite $Cu_2ZnSn(S_xSe_{1-x})_4$ quinary alloys are studied for x composition ranging from 0 to 1 with a step of 0.125. Based on first principle calculations within WIEN2K computational code the electronic band gap, band structures, CZTS-CZTSe band alignment total and partial density of states, the dielectric function and the absorption coefficient are carefully calculated and discussed.

2. Computational background

Several electronic structure computational codes are currently available and widely distributed in both research and industry. For these calculations we used the all-electron FP-LAPW+lo method, implemented in the WIEN2k computational code [22,23]. This one allows calculating the energy of the ground state and the electronic structure of the periodic systems by employing the density functional theory (DFT) in conjunction with the Kohn and Sham (KS) equations. The revised generalized gradient approximation with the exchange-correlation functional of Perdew-Burke-Ernzerhof (GGAPBEsol) [24] and the Tran-Blaha modified Becke-Johnson exchange potential (TB-mBJ) [25] approximation are used in this study. The TB-mBJ is developed to solve the problem of underestimation of band-gaps. In a more rigorous treatment and in order to improve the description of the localized semi-core 3d-states for the considered materials, the modified Becke-Johnson potential plus an on-site Coulomb U was also used in this regard. Results concerning comparisons of GGAPBEsol, TB-mBJ and TB-mBJ+U will be discussed below. The random phase approximation (RPA) dielectric function [26] are applied for evaluating optical constants taking into account inter-band contributions. The ground state electronic configuration for Zinc (Zn) atom is [Ar] $3d^{10}$ $4s^2$, Coper (Cu) is [Ar] $3d^{10}$ $4s^1$, Tin (Sn) is [Kr] $4d^{10}$ $5s^2$ $5p^2$, Sulfur (S) is [Ne] $3s^2$ $3p^4$ and the selenium (Se) atom is [Ar] $3d^{10}$ $4s^2$ $4p^4$. The electrons in closed shells are treated as core electrons whereas the rest of electrons are selected as valence states. Since the FP-LAPW is a variational method, the Kohn and Sham (KS) equations are solved in practice using the self-consistent field method (SCF). To achieve convergence of energy eigenvalues the maximum l values for partial waves used inside atomic spheres (lmax) is fixed to 10 and a value of 12 is chosen for the maximum magnitude GMAX of largest vector in charge density Fourier expansion. Also in WIEN2K computational code, core electrons are assumed to not interact. A separating energy of −6.0 Ry is used to separate core from valence states. The matrix size for convergence Rmt*Kmax is fixed as 7 and we used the atomic sphere radius (muffin-tin radius) of 2.050, 2.050, 2.40, 2,00 and 2.10 a.u. for Zn, Cu, Sn, S and Se atoms, respectively. The calculations are carried out with $12 \times 12 \times 12$ grid in the irreducible Brillouin zone equivalent to 2000 k-point meshes.

3. Results and discussions

3.1. Band gap energies

This work is part of the continuation of our previous study carried out on the structural and thermodynamic properties of $Cu_2ZnSn(S_xSe_{1-x})_4$ solid solution [27]. This present work consists in determining by electronic structure calculations based on DFT+U, the energy band gap, CZTS-CZTSe band alignment, the complex dielectric function and the absorption coefficient. A primitive stannite cell is used to construct the super cell. In order to substitute S atom by Se and obtain the distinct compositions we constructed a super-cell with 64 atoms in primitive cell (128 atoms in conventional cell).

The quinary alloys $Cu_2ZnSn(S_xSe_{1-x})_4$ is formed by five elements; Cu of group I (+1 valence), Zn of group II (+2 valences), Sn of group IV (+4 valences), and S and Se of group VI (−2 valences). The cations (Cu, Zn, Sn) are fixed and the anions (S, Se) are randomly distributed and for each distribution the energy of system is calculated to conclude the most stable configuration [27]. The obtained compositions are; 0, 0.125, 0.25, 0.375, 0.5, 0.625, 0.75, 0.875 and 1. The present electronic and optical calculation are obtained by using our previous values (Table 1) for the lattices parameters *a* and *c* predicted at 300 K by using the FP-LAPW along with quasi-harmonic model [27]. However, the modeling of electronic and optical properties could not to be complete without taking into account the relaxation effects, an inseparable effect of most theoretical calculations by first principle.

Generally speaking, the semi-local potential TB-mBJ approximation seems very promising for the estimation of band gap energy, because it reproduces in an exact way or almost the form of the OEP exchange potential of the atoms. In our TB-mBJ calculations we used the parameter of $\alpha = 0.267$, $\beta = 0.656$ bohr and $e = 1$ as improved by Koller et al. [28]. Table 2 present the calculated band gap energies for different compositions. In view of all results, the obtained ones from GGAPBESol are inconclusive, and suggest rather large errors in direct comparison with the experimental values, and give practically a zero gap for all materials. TB-mBJ approximation improves the results, reducing the average absolute error to 62% (for CTZS) compared to the GGAPBESol approximation. This improvement is not surprising since the parameters of this functional have been optimized to minimize errors on the energy gap. However, the very good performances provided by this approach remain to be emphasized. As expected by several computational studies, this semi-local functional gives qualitatively wrong results for solids which contain localized 3*d* or 4*f* electrons. The electronic correlations are too important to be treated in the strict framework of the DFT, and an electrostatic repulsion parameter U (Coulomb interaction) is added to the DFT potential for the orbitals *d* in order to obtain good band gap energy. The TB-mBJ plus the Hubbard U correction (TB-mBJ+U) approach is used here to overcome this problem with the considered Cu/Zn based-systems [29]. The Coulomb U for Cu-*3d* and Zn-*3d* orbitals is set to 4.0 and 7.5 eV, respectively. The chosen values for U are taken from literature [30,31] and are proven to give reliable description of band structures for both ternary and quaternary Cu-based semiconductors with moderate band gaps.

Taking CZTS as example, the band gap predicted with the Hubbard U correction (TB-mBJ+U), increases to 0.993 eV, in agreement with experiment (1.45[36], 1.49[47], 1.5[33], 1.38[38]) than TB-mBJ.

Comparing the results between CZTS and CZTSe, as viewed in experimental measurements, our calculation confirmed that the band gap of CZTS is greater by about ~40% than of CZTSe. Speaking about the variation of the ratio [S]/([S]+[Se]), the reduction in the size of crystalline structure influenced by the substitution of the sulfur atom by the selenium induce evolution of the electronic band gap. The values of the calculated energy band gap are found to be depending on the lattice parameter and the relaxation effect. The relaxation leads to deformations of crystalline structures of materials that induce a change in energy levels.

The composition-dependent band gap energies in CZTSSe alloys for relaxed structures is showed in Fig. 1 together with some experimental values available in the literature for these considered x composition. The band gap predicted by TB-mBJ+U method is approximately follow the quadratic equations

$$Eg^{TB-mBJ+U}_{Cu_2ZnSn(SxSe1-x)_4} = 0.60778 + 0.30451x + 0.079x^2 \quad (1)$$

The results in Fig. 1 from TB-mBJ+U approach show that the variation in band gap energy as a function of sulfur content in $Cu_2ZnSn(S_xSe_{1-x})_4$ exhibits a very small negative deviation from linear variation of Vegard's. The deviation is characterized by bowing parameter *b*, computed by appropriate fitting of the non-linear variation of the calculated band gap to the Eq. 1. In view of results presented in Fig. 1, the calculations confirm a nearly linear variation of the band gap along with the variation of chalcogens ratio, with an optical bowing parameter of 0.079 eV for our relaxed 64-based structures. Synthesis of the CZTSSe alloy by He et al. [40] resulted in almost linear bandgap dependence with a bowing parameter between 0.08 eV and 0.19 eV [41]. Our predicted result for band gap bowing parameter is therefore in excellent agreement with the experimental data. Although the precise determination of the optical bowing parameter should take into account other physical effects by considering the influence of hydrostatic pressure, the charge-transfer effect and the structural bond-length and bond-angle relaxation. A theoretical analysis of these effects on the optical bowing parameter by use of self-consistent band-structure techniques was proposed by Zunger et al. [42].

Table 1
The optimized GGAPBESol lattices parameters for different x compositions at 300 K [27] used to calculate the electronic and optical properties.

x →	0	0.125	0.25	0.375	0.5	0.625	0.75	0.875	1
Relaxa(Å) *c*	5.669	5.601	5.578	5.541	5515	5.490	5.455	5.419	5.423
(Å)	11.311	11.181	11.138	11.065	11,020	10.972	10.903	10.836	10.848

Table 2
Our calculated band gap energies for $Cu_2ZnSn(S_xSe_{1-x})_4$ within the four functional approximations. The calculated values are for relaxed structures within lattice parameters predicted at 300 K. The values in bold character are for the experimental data. For comparison we added also our calculation for 8-atom of end compounds.

Compositions	*GGAPBEsol (eV)*	*TB-mBJ (eV)*	*TB-mBJ+U (eV)*	*TB-mBJ+U with RMSE*	*Other results*
Se_4	0.000	0.272	0.614	1.043	0.9[1] 0.96[2] 1.017[3] 0.47[4]
$(S_{0.125}Se_{0.875})_4$	0.000	0.333	0.633	1.062	–
$(S_{0.25}Se_{0.75})_4$	0.000	0.377	0.692	1.121	1.08[2]
$(S_{0.375}Se_{0.625})_4$	0.000	0.418	0.738	1.167	–
$(S_{0.5}Se_{0.5})_4$	0.000	0.460	0.792	1.221	1.25[2]
$(S_{0.625}Se_{0.375})_4$	0.000	0.474	0.810	1.239	–
$(S_{0.75}Se_{0.25})_4$	0.000	0.541	0.889	1.318	–
$(S_{0.875}Se_{0.125})_4$	0.000	0.577	0.931	1.360	–
S_4	0.000	0.573	0.993	1.422	1.45[5] 1.49[6] 1.5[2] 1.38[7] 1.55[8]

[1]Ref. [32], [2]Ref. [33](for x = 0, 0.23, 0.49 and 1), [3]Ref. [34], [4]Ref. [35], [5]Ref. [36], [6]Ref. [37], [7]Ref. [38], [8]Ref.[39]

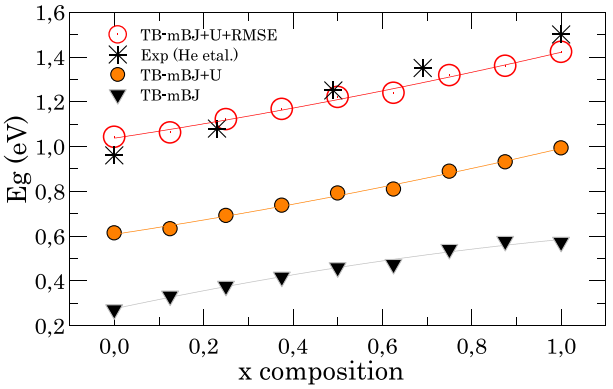

Fig. 1. Bandgap calculated with TB-mBJ and TB-mBJ+U approximations as a function of x for $Cu_2ZnSn(S_xSe_{1-x})_4$ alloys. The corrected band gap with the experimental results of He et al. [33] via the root mean squared error (RMSE) is also added. The solid lines are polynomial fits to the data. The experimental data are from He et al. [33].

To determine the standard deviation from the experimental results we used the root mean squared error (RMSE) that represents the differences between the predicted results and the experimental values. The RMSE here is defined by [43].

$$RMSE = \sqrt{\frac{1}{N_{sample}} \sum_{i=1}^{N_{sample}} \left(A^{i,calc} - A^{i,\exp}\right)^2} \tag{2}$$

where A is the considered quantity, N_{sample} is the number of compounds. In our case, we have 4 experimental values, 0.96, 1.08, 1.25 and 1.5 eV, respectively for x = 0, 0.23, 0.49 and 1 [33]. The calculated RMSE for our materials are 0.4292 eV for relaxed structures. The predicted energy band gap (Eg) with the root mean squared error (RMSE) become

$$Eg^{\mathrm{TB-mBJ+U}\,with RMSE}_{Cu_2ZnSn(SxSe1-x)_4} = 1.0369 + 0.30451x + 0.0789x^2 \tag{3}$$

In Fig. 1 we give the calculated band gap parameter for stoichiometric mixed-anion corrected with root mean squared error (RMSE) by using experimental results of He et al. [33].

3.2. *Electronic band structure and partial densities of states*

The electronic band structures calculated with the TB-mBJ+U method for $Cu_2ZnSnSe_4$, $Cu_2ZnSn(S_{0.5}Se_{0.5})_4$ and Cu_2ZnSnS_4 along the high-symmetry lines of the first Brillouin zone are shown in Fig. 2. For convenience, the energy Fermi is taken at 0 eV. The Fermi energy is by definition the energy of the highest occupied state at 0 K.

The selected high-symmetry k-points (crystal coordinates with respect to reciprocal primitive vectors) for the electronic band structure calculation are shown in Fig. 3 and the values are summarized in Table 3. From the calculated TB-mBJ+U band structures, all our materials have a direct fundamental band gap at Γ in the first Brillouin zone. It is also interesting to pay our attention on the densities of the electronic states and, therefore, on the contribution of each orbitals on the band structure. The electron density of states of a crystalline material can be described as the statistical contribution of each energy level that can be occupied in a particular energy range. According to the electronic densities of states calculations (DOS) presented in Fig. 2 and calculated with TB-mBJ+U

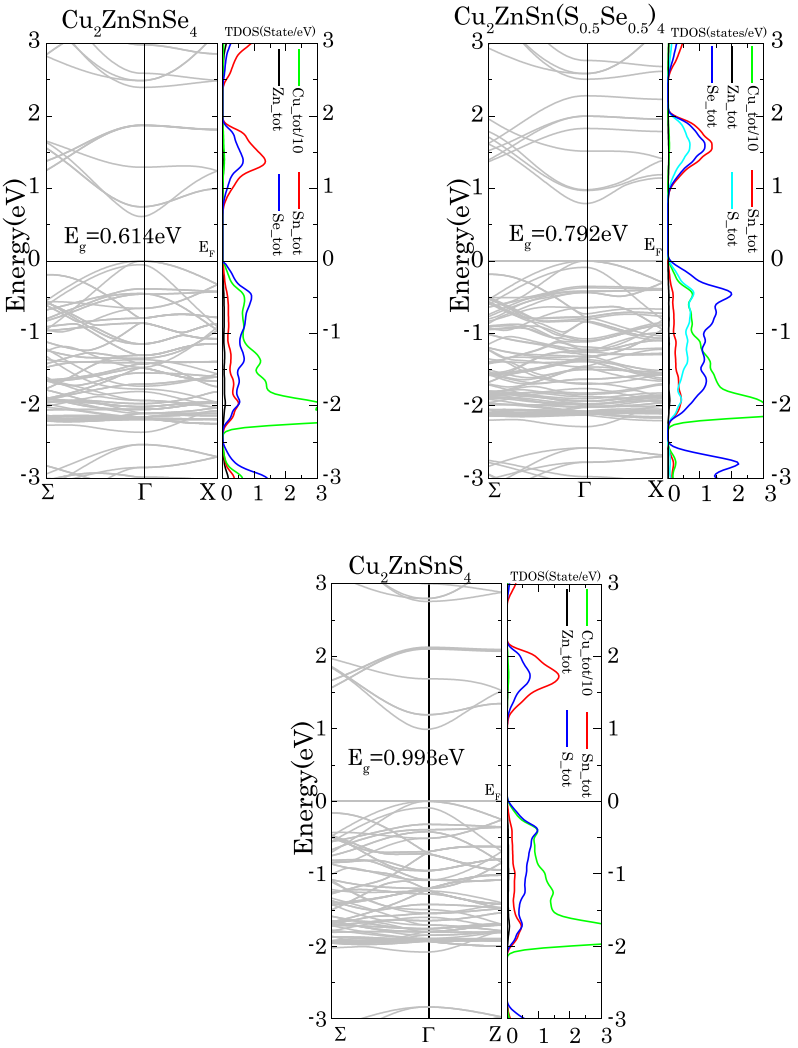

Fig. 2. Calculated TB-mBJ+U band structures and total densities of states of $Cu_2ZnSnSe_4$, $Cu_2ZnSn(S_{0.5}Se_{0.5})_4$ and Cu_2ZnSnS_4 relaxed materials. In the figures, the Cu_tot states is devided per 10. The total DOS is given in States/eV.

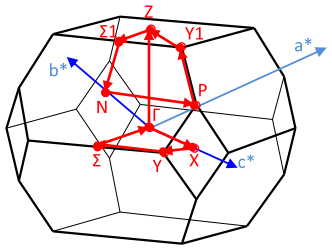

Fig. 3. Brillouin zone of Cu_2ZnSnS_4 in crystalized in Body-centered tetragonal with different symmetry k-points. The structure is made using XCrySDen visualization program [44]. The coordinates of symmetry k-points are given in fractions of the primitive reciprocal lattice vectors a*, b* and c*.

approximation, the top of valence bands is mainly composed of Cu_3d and Se_4p hybridized anti-bonding states for $Cu_2ZnSnSe_4$, Cu_3d and S_3p for Cu_2ZnSnS_4, and for $Cu_2ZnSn(S_{0.5}Se_{0.5})_4$ we noted a mixture of Cu_3d, S_3p and Se_4p states. The Cu_3d states are very shallow with high eigen energy for all materials. The bottom of the conduction band is mainly formed by Sn_5s and Se_4p for CZTSe, and Sn_5s / Se_4p / S_3p for $Cu_2ZnSn(S_{0.5}Se_{0.5})_4$, and Sn_5s with S_3p for CZTS. The Sn_5s, Se_4p, and S_3p levels shift up in order (from x = 0–1), which caused to shift the conduction band minimum (CBM) level to the up and increases the band gap in order (from

Table 3
Symmetry k-points of Cu_2ZnSnS_4 in stannite structure I-42 m with body-centered tetragonal. In relation (4), *a* and *c* represent the lattice parameter of the structure [45].

_a*	_b*	_c*	Symmetry k-points
0.00000	0.00000	0.00000	Γ
0.00000	0.00000	0.50000	X
-0.12495 (-ζ)	0.12495 (+ζ)	0.50000	Y
-0.31248 (-υ)	0.31248 (+υ)	0.31248 (+υ)	Σ
0.00000	0.00000	0.00000	Γ
0.50000	0.50000	-0.50000	Z
0.31248 (+υ)	0.68753 (1-υ)	-0.31248 (-υ)	Σ1
0.00000	0.50000	0.00000	N
0.25000	0.25000	0.25000	P
0.50000	0.50000	-0.12495 (-ζ)	Y1
0.50000	0.50000	-0.50000	Z

x = 0–1). Also, the partial DOS shows that the Sn_5s state is much stronger than Se_4p, and S_3p.

$$\text{Where} \upsilon = \frac{(1 + a^2/c^2)}{4} \text{and} \xi = \frac{a^2}{2c^2} \tag{4}$$

3.3. Band alignment between CZTS and CZTSe

Fig. 4, shows a comparison of the band alignment between CZTS and CZTSe predicted for both TB-mBJ and TB-mBJ+U approximations. In view of all these results, it is undeniable that the TB-mBJ+U approximation has completely changed the shape of the band alignment. Taking the CZTS compound as an example, based on our TB-mBJ+U approximation, the Fermi level decreased to a value equal to 0.3708Ryd (E_F= 0.4036Ryd with TB-mBJ) and the valence band maximum state is pushed up. With this shift, the minimum conduction band was also upward moved, which explains the increase in the band gap energy from 0.573 (TB-mBJ) to 0.993 with TB-mBJ+U. The same thing was noted for the CZTSe. With regard to the band alignment between CZTS and the CZTSe compounds, based on TB-mBJ+U calculations, the Ec offset (CBO~0.2716 eV) is larger than the Ev offset (VBO~0.1074 eV) in agreement with other theoretical calculation of Chen et al. [46] (CBO ~ 0.35 eV and VBO ~ 0.15 eV) and the experimental results of Haight et al. [47] (CBO ~ 0.3 eV and VBO ~ 0.2 eV). The predicted TB-mBJ+U results confirm also that the x variation has more important effect on the Ec rather than Ev within the application of Hubbard U correction.

3.4. Linear optical properties

The optical properties are among the most important characteristics and knowledge of these properties for such material plays an important role especially in the development of solar cells with high efficiency. The optical properties of a material are described by the quantity of photons that can be absorbed by this material. There are several useful optical parameters to be considered when characterizing an optoelectronic material. Listed in the order of most fundamental optical quantities; the absorption coefficient, the

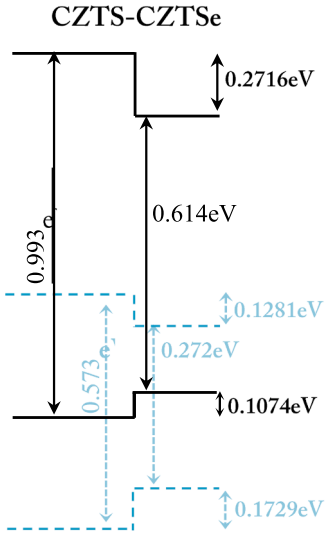

Fig. 4. Band alignment between CZTS and CZTSe calculated for both TB-mBJ (dashed-blue) and TB-mBJ+U (black) approximations.

complex index of refraction, and the reflectivity [48]. In this section, we shall examine the dielectric function and the absorption coefficient and demonstrate their inter relationship with x composition and the band gap energy. A uniform 0.1 eV broadening is used for all alloys and a scissors correction shift of 0.429 eV are applied to adjust the inter-band optical transitions in the materials.

3.4.1. Dielectric functions

The complex dielectric function is introduced through Maxwell's equations. The microscopic dielectric function is the basic quantity that gives information about the screening of the system in the linear response, and is closely related to the electronic band structure of the material [49–51]. The imaginary part of the dielectric function takes the following form

$$\varepsilon_2(\omega) = \frac{e^2\hbar}{\pi m^2\omega^2}\sum_{c,v}\int_{BZ}|M_{cv}(k)|^2\delta[\omega_{cv}(k)-\omega]d^3k \tag{5}$$

The dielectric function parts are not independent and the real quantity can be obtained from the imaginary one by means of Kramers-Kronig transformation [52]. The general expression of $\varepsilon_1(\omega)$ is given by

$$\varepsilon_1(\omega) = 1+\frac{2}{\pi}p\int_0^{\infty}\frac{\omega'\varepsilon_2(\omega')}{\omega' 2-\omega^2}d\omega' \tag{6}$$

The light is described by a transverse wave. For the anisotropic media as in tetragonal materials, the optical constants may be different for the two polarization directions.

The real and imaginary parts of dielectric constant depend on polarization of light in the materials. In order to see the degree of the anisotropy in our materials, we first considered the spectrum of dielectric function calculated using the TB-mBJ + U + Δ_E for the parent compounds (CZTS and CZTSe). From figure the materials are anisotropic in this stannite structure, with the dielectric response along *z* being different from that along *x axe* (x = *y* axe). The dielectric tensor is sensitive to the plane of incidence.

This stannite structure showed that both ordinary and extraordinary dielectric functions are not the same. The result indicates that

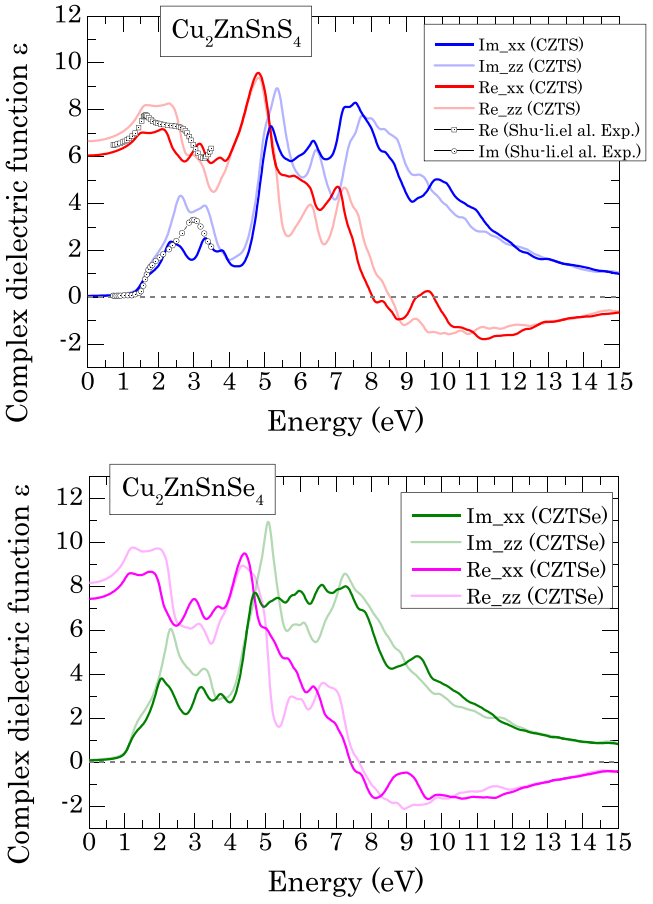

Fig. 5. Real and imaginary parts of the frequency dependent dielectric function along xx and zz axis ($E^{\perp}c^*$ and $E//c^*$ polarization) for Cu_2ZnSnS_4, and $Cu_2ZnSnSe_4$ compounds. The experimental real and imaginary parts of dielectric function determined by ellipsometry are taken from Shu-yi et al. [39].

the materials are positive birefringent.

From the graphs of Fig. 5, it is clear that both real and imaginary part of dielectric constant increases with increase of photon energy and decrease when it reaches the maximum value. As a general comment, the imaginary part of dielectric function appears as extremely very slow in the infrared region. In the range of 0–4 eV, we added the experimental real and imaginary parts of ε(ω) of CZTS determined by ellipsometry by Shu-yi et al. [39]. In this region, our results present good agreement with experimental observation of Shu-yi et al.

The dielectric function spectrum for all compositions along xx and zz axis ($E^{\perp}c^*$ and $E//c^*$ polarization) is presented in Figs. 6 and 7 for energies from 0 to 20 eV. A careful look at this figure clearly shows six major critical points CPs denoted as Ej (E0-E5). The critical points are the direct band-to-band transition at the points of high symmetry band gap. The first critical point E_0 is transition between the highest valence band and the lowest conduction bands at Γ (fundamental absorption edge). Our analysis show values of 1.48 eV and 1.53 eV, respectively for E_0_xx and E_0_zz, in agreement with the reported one of 1.6 eV in Ref. [39].

From our band structure calculated with TB-mBJ+U we find that the critical point E1 is originates from direct transition from the uppermost valence band to the lowest conduction band around the X point of the Brillouin zone. As general comment, it is clear that the critical points (CPs) slightly-shift toward higher energy as sulfur content increases. Also, the partial substitution of Se by S leads to a decrease of the CPs values.

In order to obtain analytic static values of ε with x composition, we can fit the calculated values to the quadratic polynomial function. The results approximately follow the quadratic equations

$$\varepsilon_1(0)\begin{cases} \_xx = 7.4541 - 1.1169x - 0.2679x^2 \\ \_zz = 8.1845 - 1.2442x - 0.2555x^2 \end{cases} \tag{7}$$

Fig. 8 shows the S-composition dependences of static dielectric function.

3.4.2. Absorption coefficient

The absorption coefficient is the main visualization quantity in materials science, because it allows predicting the usefulness of such

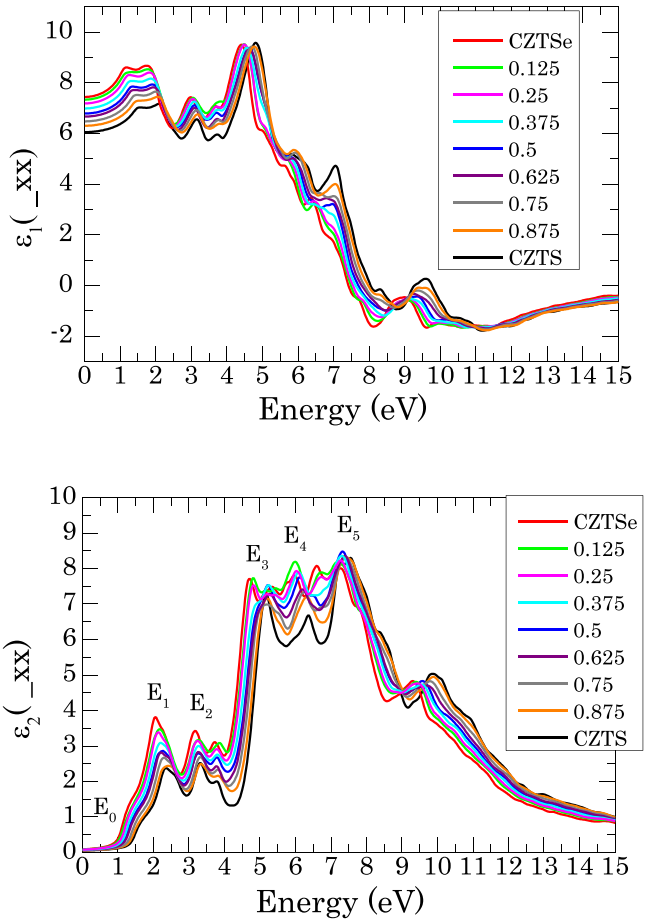

Fig. 6. Real and imaginary parts of the frequency dependent dielectric function along xx axis ($E^{\perp}c^*$) for $Cu_2ZnSn(S_xSe_{1-x})_4$. CPs energies are showed and denoted as Ej.

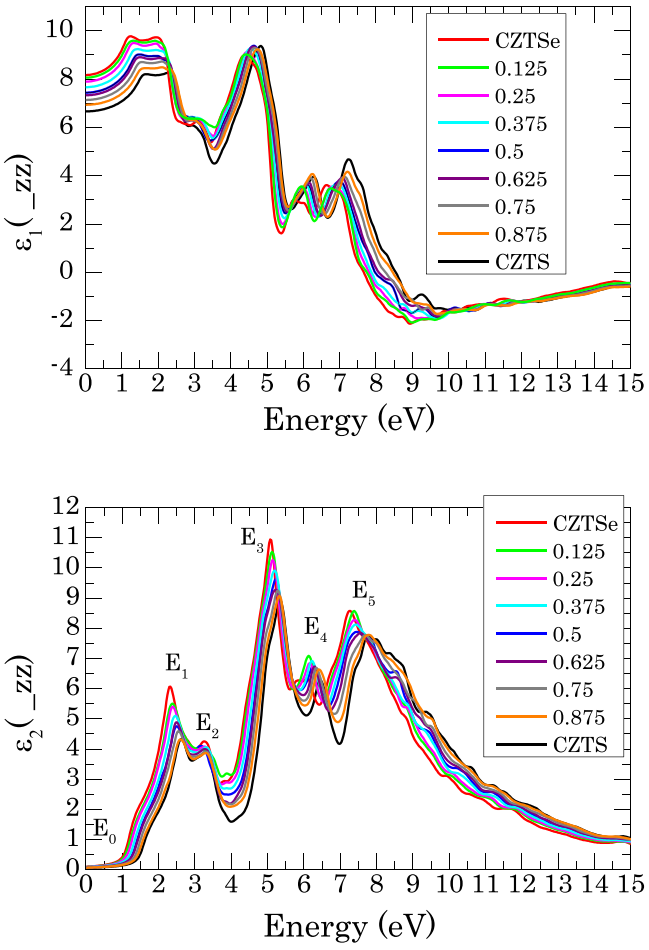

Fig. 7. Real and imaginary parts of the frequency dependent dielectric function along zz axis (E//c* polarization) for $Cu_2ZnSn(S_xSe_{1-x})_4$. Critical points (CPs) energies are showed and denoted as Ej.

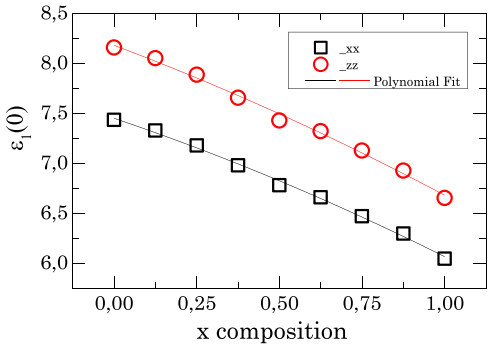

Fig. 8. Composition dependences of the static real parts of the dielectric function along xx and zz axis. The open square/circle are the calculated values and the solid lines are fit by Eq. (7).

a material in an optoelectronic application. The absorption coefficient is calculated by the following relationship

$$\alpha(\omega) = \frac{2\omega}{c}.k \tag{8}$$

Where c is the speed of light in vacuum and k is the imaginary part of the refractive index.

The optical absorption is generated from the dielectric function. The spectra are presented with an energy shift of 0.429 eV (scissor

operator). Fig. 8 displays the absorption coefficient profiles against the incident photon energy for all composition in $Cu_2ZnSn(S_xSe_{1-x})_4$. As we can see from the figure, the shape of the absorption curves is almost similar, with a slight shift of the main peaks. The optical absorption starts with feeble absorption in the visible range (from 680 to 390 nm) and increase to a very intense one at high energy in ultra violet region ($\leq$ 380 nm). The fundamental absorption edge and the most intense absorption peak shift towards to high energy side with increasing S content in $Cu_2ZnSn(S_xSe_{1-x})_4$. From 0.5–3 eV, CZTSe have higher absorption compared with that of CZTS. Contrariwise the most intense absorption peak for CZTS is appearing in higher intensity than for CZTSe (Fig. 9).

4. Conclusion

The bulk solid solution $Cu_2ZnSn(S_xSe_{1-x})_4$ has been studied experimentally by a limited number of researchers [20,21,33]. These experiments make it possible to explain the variation of the lattice constants and band gap energy as a function of x composition. The purpose of this study is to improve the understanding of the evaluation of these constants as a function of x within the ab-initio method. In this study, we continued our work focused on the structural and thermodynamic properties of alloys derived from a mixed sulfur/selenium [27]. We will focus here not only on the evolution of the energy band gap as a function of the substitution rate but will also try to understand the optical quantities in this solid solution. The band gap energy is the minimum energy necessary to elevate an electron to the excited state.

The inspection of the results reveals that the used functional could not exactly reproduce the experimental band gap energy. Beyond the error made by the exchange and correlation functional, the static DFT calculations neglect the energetic contributions resulting from the movement of atoms. Also, saying that our systems contain elements of 3d based-electrons, we used the TB-mBJ+U approximation in order to treat the strong on-site Coulomb interaction of these localized electrons on energy band gap, with an additional Hubbard-like U term. As results, even with the addition of U parameter, the TB-mBJ+U band gap is improved compared to TB-mBJ, but the correction is not sufficient to obtain the full agreement with the experiment. It is worth noting also that our calculations reproduce qualitatively the T = 0 K electronic and optical properties. Noted, the materials simulated here are perfectly monocrystalline without any structural defects. If we consider all results published previously, it clearly appears that band gap energies differ significantly from one study to another. Experimentally, the energy gap is influenced by other parameters such as the

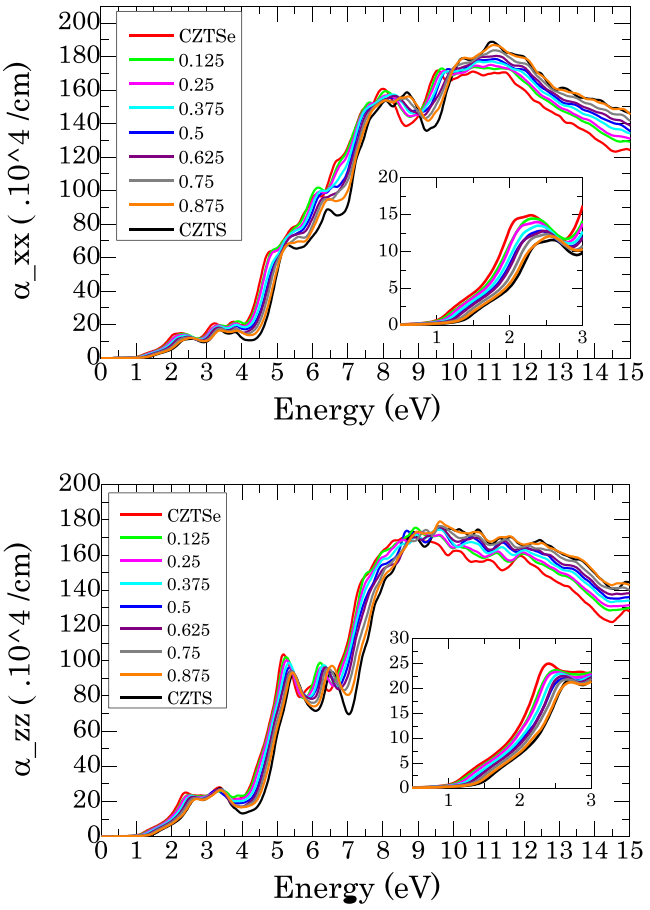

Fig. 9. The calculated absorption coefficient as a function of x for $Cu_2ZnSn(S_xSe_{1-x})_4$ alloys along xx and zz axis.

stoichiometry deviation, the cationic disorder on the structure and the annealing effect on the sample, and if the latter is soaked or cooled very slowly [18]. The energy band gap appears decisive with regard to the optical properties and therefore requires a fine determination in order to be able to define the limits of application of each compound. For a material to be a potential candidate for solar cell applications, absorption coefficient must be kept as high as possible. The complex dielectric function (real and imaginary parts, ε_1 and ε_2) for $Cu_2ZnSn(S_xSe_{1-x})_4$ obtained from TB-mBJ + U + Δg is presented.

From the results reported in this work, the substitution of S by Se induces an increase in the energy band gap, and a decrease in the absorption coefficient in the visible region of the optical spectrum.

Declaration of Competing Interest

We wish to confirm that there are no known conflicts of interest associated with this work.

Acknowledgements

The authors are deeply grateful to all collaborators who participated in this work. Also, we are grateful to TUAN V. VU from Ton Duc Thang (University of Vietnam) for their valuable and useful discussions about DFT+U.

References

[1] A.V. Baranov, T.A. Stolyarova, E.A. Brichkina, E.G. Osadchii, Standard enthalpy of the formation of selenium stannite Cu2FeSnSe4, Geochem. Int. 57 (2019) 1120–1123.
[2] Yi-Ping Wang, Sergiu Levcenco, Dumitru O. Dumcenco, Ying-Sheng Huang, Cing-Hwa Ho, Kwong-Kau Tiong, Composition dependent band gaps of single crystal Cu2ZnSn(SxSe1-x)4 solid solutions, Solid State Phenom. 194 (2013) 139–143.
[3] Kentaro Ito, Tatsuo Nakazawa, Electrical and optical properties of stannite-type quaternary semiconductor thin films, Part 1, Jpn. J. Appl. Phys. 27 (11) (1988) 2094–2097.
[4] Shin Tajima, Mitsutaro Umehara, Masaki Hasegawa, Takahiro Mise, Tadayoshi Itoh, Cu2ZnSnS4 photovoltaic cell with improved efficiency fabricated by high-temperature annealing after CdS buffer-layer deposition, Prog. Photo. Res. Appl. (2016).
[5] Se.Jin Ahn, Sunghun Jung, Jihye Gwak, Ara Cho, Keeshik Shin, Kyunghoon Yoon, Doyoung Park, Hyeonsik Cheong, Jae Ho Yun, Determination of band gap energy (Eg) of Cu2ZnSnSe4 thin films: on the discrepancies of reported band gap values, Appl. Phys. Lett. 97 (2010), 021905.
[6] Silvana Botti, David Kammerlander, Miguel A.L. Marques, Band structures of Cu2ZnSnS4 and Cu2ZnSnSe4 from many-body methods, Appl. Phys. Lett. 98 (2011), 241915.
[7] B.D. Chernomordik, A.E. Béland, N.D. Trejo, A.A. Gunawan, D.D. Deng, K.A. Mkhoyan, E.S. Aydil, Rapid facile synthesis of Cu2ZnSnS4 nanocrystals, J. Mater. Chem. A 2 (2014) 10389–10395.
[8] Hironori KATAGIRI, Naoya ISHIGAKI, Takeshi ISHIDA, Kotoe SAITO, Characterization of Cu2ZnSnS4 thin films prepared by vapor phase sulfurization, Jpn. J. Appl. Phys. 40 (2001) 500–504.
[9] H. Matsushita, T. Ichikawa, A. Katsui, Structural, thermodynamical and optical properties of Cu2-II-IV-VI4 quaternary compounds, J. Mater. Sci. 40 (2005) 2003–2005.
[10] G. Brammertz, M. Buffière, S. Oueslati, H. ElAnzeery, K. Ben Messaoud, S. Sahayaraj, C. Köble, M. Meuris, J. Poortmans, Characterization of defects in 9.7% efficient $Cu_2ZnSnSe_4$-CdS-ZnO solar cells, Appl. Phys. Lett. 103 (2013), 163904.
[11] Fangyang Liu, Fangqin Zeng, Ning Song, Liangxing Jiang, Zili Han, Zhenghua Su, Chang Yan, Xiaoming Wen, Xiaojing Hao, Yexiang Liu, Kesterite Cu2ZnSn(S, Se)4 solar cells with beyond 8% efficiency by a Sol-Gel and selenization process, ACS Appl. Mater. Interfaces 7 (2015) 14376–14383.
[12] Wei Wu, Nancy G. Tassi, Yanyan Cao, Jonathan V. Caspar, Kaushik Roy-Choudhury, Lei Zhang, Optoelectronic characteristics of >9% efficient bilayered CuZnSn(S,Se)4 photovoltaic device, Phys. Status Solidi RRL (2015) 1–5.
[13] Nathaniel J. Carter, Charles J. Hages, James E. Moore, Steven M. McLeod, Caleb K. Miskin, Chinmay Joglekar, Mark S. Lundstrom, Rakesh Agrawal, Analysis of temperature-dependent current-voltage characteristics for CIGSSe and CZTSSe thin film solar cells from nanocrystal inks, IEEE 39th Photovoltaic Specialists Conference (PVSC), Tampa, FL (2013) 3062–3065.
[14] J.K. Larsen, Y. Ren, N. Ross, E. Sarhammer, S.-Y. Li, C. Platzer-Bjorkman, Surface modification though air annealing Cu2ZnSn(S,Se)4 absorbers, Thin Solid Films 633 (1 July) (2017) 118–121.
[15] D. Aaron, R. Barkhouse, Oki Gunawan, Tayfun Gokmen, Teodor K. Todorov, David B. Mitzi, Device characteristics of a 10.1% hydrazine-processed $Cu_2ZnSn(Se, S)_4$ solar cell, Prog. Photo. Res. Appl. 20 (2012) 6–11.
[16] Kee-Jeong Yang, Dae-Ho Son, Shi-Joon Sung, Jun-Hyoung Sim, Young-Ill Kim, Si. Nae Park, Dong-Hwan Jeon, JungSik Kim, Dae-Kue Hwang, Chan-Wook Jeon, Dahyun Nam, Hyeonsik Cheong, Jin-Kyu Kang, Dae-Hwan Kim, A band-gap graded CZTSSe solar cell with 12.3% efficiency, J. Mater. Chem. A 4 (2016) 10151–10158.
[17] Wei Wang, Mark T. Winkler, Oki Gunawan, Tayfun Gokmen, Teodor K. Todorov, Yu Zhu, B. Mitzi David, Device characteristics of CZTSSe thin-film solar cells with 12.6% efficiency, Adv. Energy Mater. (2013).
[18] Pierre Bais, Maria Teresa Caldes, Michae Paris, Catherine Guillot-Deudon, Pierre Fertey, Bernadette domengès, and alain lafond, cationic and anionic disorder in CZTSSe kesterite compounds: a chemical crystallography study, Inorg. Chem. 56 (19) (2017) 11779–11786.
[19] Mohamed Issam Ziane, Meftah Tablaoui, Amar Khelfane, Moufdi Hadjab, Hamza Bennacer, Optoelectronic properties of the new quaternary chalcogenides $Zn_2CuInTe_4$ and $Cd_2CuInTe_4$: ab-initio study, Optik 157 (2018) 248–258.
[20] Keng-Liang Ou, Jian-Cin Fan, Jem-Kun Chen, Chih-Ching Huang, Liang-Yih Chen, Jinn-Hsuan Ho, Jia-Yaw Chang, Hot-injection synthesis of monodispersed Cu2ZnSn(SxSe1-x)4 nanocrystals: tunable composition and optical properties, J. Mater. Chem. 22 (2012) 14667–14673.
[21] Akira Nagaoka, Kenji Yoshino, Hiroki Taniguchi, Tomoyasu Taniyama, Koichi Kakimoto, Hideto Miyake, Growthandcharacterization of Cu2ZnSn(SxSe1_x)4 alloysgrown by the melting method, J. Cryst. Growth 386 (2014) 204–207.
[22] Karlheinz Schwarz, Peter Blaha, Solid state calculations using WIEN2k, Comput. Mater. Sci. 28 (2003) 259–273.
[23] Peter Blaha, Karlheinz Schwarz, Fabien Tran, Robert Laskowski, Georg K.H. Madsen, Laurence D. Marks, WIEN2k: An APW+lo program for calculating the properties of solids, J. Chem. Phys. 152 (2020), 074101.
[24] J.P. Perdew, A. Ruzsinszky, G.I. Csonka, O.A. Vydrov, G.E. Scuseria, L.A. Constantin, X. Zhou, K. Burke, Restoring the density-gradient expansion for exchange in solids and surfaces, Phys. Rev. Lett. 100 (2008), 136406.
[25] Fabien Tran, Peter Blaha, Accurate Band Gaps of Semiconductors and Insulators with a Semilocal Exchange-Correlation Potential, Phys. Rev. Lett. 102 (2009), 226401.
[26] Claudia Ambrosch-Draxl, Jorge O. Sofo, Linear optical properties of solids within the full-potential linearized augmented planewave method, Comput. Phys. Commun. 175 (2006) 1–14.

[27] Mohamed Issam Ziane, Djamel Ouadjaout, Meftah Tablaoui, Rachida Nouri, Wafia Zermane, Abdelkader Djelloul, Hamza Bennacer, Abderrahmane Mokrani, Moufdi Hadjab, Hamza Abid, First-principle computed structural and thermodynamic properties of Cu2ZnSn(SxSe1-x)4 pentanary solid solution, J. Electron. Mater. 48 (2019) 6991–7002.
[28] David Koller, Fabien Tran, Peter Blaha, Improving the modified Becke-Johnson exchange potential, Phys. Rev. B 85 (2012), 155109.
[29] I. Vladimir, Jan Anisimov, Zaanen, Ole K. Andersen, Band theory and Mott insulators: Hubbard *U* instead of Stoner, Phys. Rev. B 44 (1991) 943–954.
[30] Yubo Zhang, Jiawei Zhang, Weiwei Gao, Tesfaye A. Abtew, Youwei Wang, Peihong Zhang, Wenqing Zhang, Near-edge band structures and band gaps of Cu-based semiconductors predicted by the modified Becke-Johnson potential plus an on-site Coulomb U, J. Chem. Phys. 139 (2013), 184706.
[31] W. Setyawan, R.M. Gaume, S. Lam, R.S. Feigelson, S. Curtarolo, High-throughput combinatorial database of electronic band structures for inorganic scintillator materials, ACS Comb. Sci. 13 (2011) 382–390.
[32] G. Zoppi, I. Forbes, R.W. Miles, P.J. Dale, J.J. Scragg, L.M. Peter, Cu2ZnSnSe4 thin film solar cells produced by selenisation of magnetron sputtered precursors, Prog. Photo. Res. Appl. 17 (2009) 315–319.
[33] Jun He, Lin Sun, Nuofan Ding, Hui Kong, Shaohua Zuo, Shiyou Chen, Ye Chen, Pingxiong Yang, Junhao Chu, Single-step preparation and characterization of Cu2ZnSn(SxSe1-x)4 thin films deposited by pulsed laser deposition method, J. Alloy. Compd. 529 (2012) 34–37.
[34] J. Krustok, R. Josepson, T. Raadik, M. Danilson, Potential fluctuations in Cu2ZnSnSe4 solar cells studied by temperature dependence of quantum efficiency curves, Phys. B 405 (2010) 3186–3189.
[35] Satoshi Nakamura, Tsuyoshi Maeda, Takahiro Wada, Phase stability and electronic structure of in-free photovoltaic materials: Cu2ZnSiSe4, Cu2ZnGeSe4, and Cu2ZnSnSe4, Jpn. J. Appl. Phys. 49 (2010), 121203.
[36] Hironori Katagiri, Nobuyuki Sasaguchi, Shima Hando, Suguru Hoshino, Jiro Ohashi, Takaharu Yokota, Preparation films by and evaluation of Cu2ZnSnS4 thin sulfurization of E-B evaporated precursors, Sol. Energy Mater. Sol. Cells 49 (1997) 407–414.
[37] Jonathan J. Scragg, Philip J. Dale, Laurence M. Peter, Guillaume Zoppi, and Ian Forbes, New routes to sustainable photovoltaics: evaluation of Cu2ZnSnS4 as an alternative absorber material, Phys. Stat. Sol. (b) 245 (No. 9) (2008) 1772–1778.
[38] Shiyou Chen, X.G. Gong, Aron Walsh, Su-Huai Wei, Crystal and electronic band structure of Cu2ZnSnX4 (X = S and Se) photovoltaic absorbers: first-principles insights, Appl. Phys. Lett. 94 (2009), 041903.
[39] Shu-yi Li, Sergiy Zamulko, Clas Persson, Nils Ross, Jes K. Larsen, Optical properties of Cu2ZnSn(SxSe1-x)4solar absorbers: spectroscopic ellipsometry andab initiocalculations, Appl. Phys. Lett. 110 (2017), 021905.
[40] Jun He, Lin Sun, Shiyou Chen, Ye Chen, Pingxiong Yang, Junhao Chu, Composition dependence of structure and optical properties of Cu2ZnSn(S,Se)4 solid solutions: an experimental study, J. Alloy. Compd. 511 (2012) 129–132.
[41] S. Levcenco, D. Dumcenco, Y.P. Wang, Y.S. Huang, C.H. Ho, E. Arushanov, V. Tezlevan, K.K. Tiong, Influence of anionic substitution on the electrolyte electroreflectance study of band edge transitions in single crystal Cu2ZnSn(SxSe1-x)4 solid solutions, Opt. Mater. 34 (2012) 1362–1365.
[42] James E. Bernard, Alex Zunger, Optical bowing in zinc chalcogenide semiconductor alloys, 15, Phys. Rev. B Condens Matter 34 (8) (1986) 5992–5995.
[43] Kousuke Nakano, Tomohiro Sakai, Assessing the performance of the Tran–Blaha modified Becke–Johnson exchange potential for optical constants of semiconductors in the ultraviolet–visible light region, J. Appl. Phys. 123 (2018), 015104.
[44] Anton Kokalj, XCrySDen—a new program for displaying crystalline structures and electron densities, J. Mol. Graph. Model. 17 (1999) 176–179.
[45] Wahyu Setyawan, Stefano Curtarolo, High-throughput electronic band structure calculations: challenges and tools, Comput. Mater. Sci. 49 (2010) 299–312.
[46] Shiyou Chen, Aron Walsh, Ji-Hui Yang, X.G. Gong, Lin Sun, Ping-Xiong Yang, Jun-Hao Chu, Su-Huai Wei, Compositional dependence of structural and electronic properties of Cu2ZnSn(S,Se)4 alloys for thin film solar cells, Phys. Rev. B 83 (2011), 125201.
[47] Richard Haight, Aaron Barkhouse, Oki Gunawan, Byungha Shin, Matt Copel, Marinus Hopstaken, David B. Mitzi, Band alignment at the Cu2ZnSn(SxSe1−x)4/CdS interface, Appl. Phys. Lett. 98 (2011), 253502.
[48] Greg P. Smestad, Optoelectronics of Solar Cells, ISBN 0-8194-4440-5, Spie Press, 2002.
[49] Mohamed Issam Ziane, Zouaoui Bensaad, Tarik Ouahrani, Hamza Bennacer, First principles study of structural, electronic and optical properties of indium gallium nitride arsenide lattice matched to gallium arsenide, Mater. Sci. Semicond. Process. 30 (2015) 181–196.
[50] Kin Mun Wong, Characterization modeling and physical mechanisms of different surface treatment methods at room temperature on the oxide and interfacial quality of the SiO2 film using the spectroscopic scanning capacitance microscopy, Results Phys. 7 (2017) 1308–1318.
[51] Kin Mun Wong, Study of the electronic structure of individual free-standing germanium nanodots using spectroscopic scanning capacitance microscopy, Jpn. J. Appl. Phys. 48 (2009), 085002.
[52] V. Lucarini, J.J. Saarinen, K.E. Peiponen, E.M. Vartiainen, Kramers-Kronig Relations in Optical Materials Research, Springer Science & Business Media, Berlin, 2005.